3rd International Symposium on the Recent Developments in Plate Steels
2–5 June 2024, Vail, Colo., USA
DOI: 10.33313/300/027

Microstructure Response to Intermediate Reheating in Hot Strip Processing

P. Uranga[1,2], U. Mayo[1,2], M. J. Merwin[3]

[1]CEIT-Basque Research and Technology Alliance (BRTA), Materials and Manufacturing Division
[2]Univ. of Navarra-Tecnun, Mechanical and Materials Engineering Department
20018 Donostia-San Sebastián, Basque Country, Spain
puranga@ceit.es; umayo@ceit.es

[3]United States Steel Corporation, Research and Technology Center
800 East Waterfront Dr., Munhall, PA 15120
mmerwin@uss.com

Keywords: Endless rolling, thermomechanical processing, microalloyed steel, microstructural evolution, modeling

INTRODUCTION

Steel production methods continue to advance in terms of energy efficiency, capital intensity, and operating costs. The direct linkage of continuous casting and hot rolling operations has proven to be very successful with many new plants adopting this configuration. Variations on the specifications for these facilities have been introduced to optimize performance for specific needs. For example, cast slab thickness has been increased and roughing mills have been introduced to improve microstructure uniformity in thicker hot-rolled strip products [1-5]. One recent mill design is the Arvedi ESP (endless strip production) process [6-8], currently under construction at U. S. Steel's Big River Steel (BRS) complex in Osceola, AR. This mill is scheduled to begin operation in 2024 [9,10]. Schematic illustrations of the mill configurations available within U. S. Steel are presented in Figure 1.

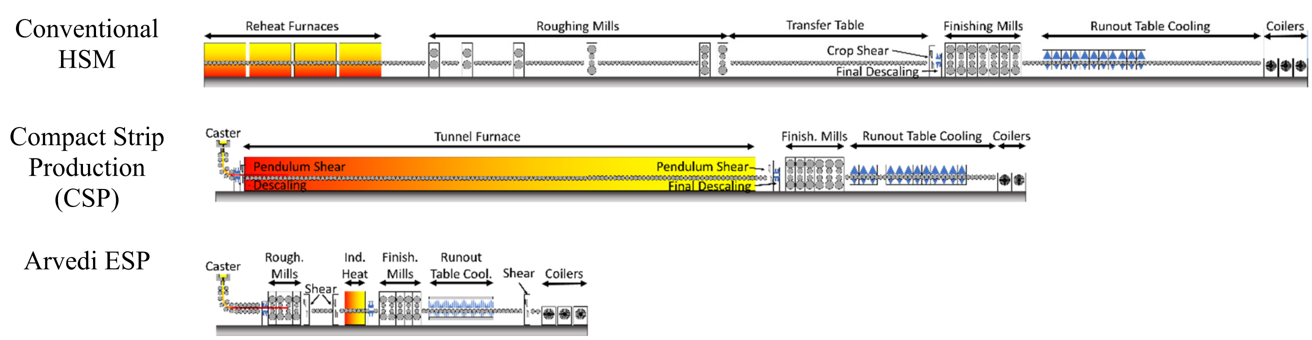

Figure 1. Schematic illustration of mill configurations within U. S. Steel. These represent a conventional hot-strip mill (*e.g.* Gary Works), a CSP mill (at BRS), and an Arvedi ESP mill (at BRS). Lengths of the schematics are roughly to scale.

The mill configurations shown in Figure 1 result in significantly different time-temperature-deformation schedules during strip production. These differences are illustrated below in Figure 2, for strip of nominally 2mm thickness that was produced on a conventional hot-strip mill (HSM), BRS's (CSP) mill, and modeled for the configuration of the new Arvedi ESP at BRS, respectively. Key distinctions between these processes include the absence of roughing deformation in the CSP mill and significant reheating of the transfer bar prior to finish rolling in the Arvedi ESP mill. An important aspect of the ESP condition is the direct linkage of the cast strand throughout the rolling process, continuing until it is sheared immediately upstream of the coiler. Consequently, the rolling speed is tied to casting speed, with mass flow during rolling generally slower than in an uncoupled case. As such, roughing temperatures can be significantly lower than in a conventional HSM and interpass times

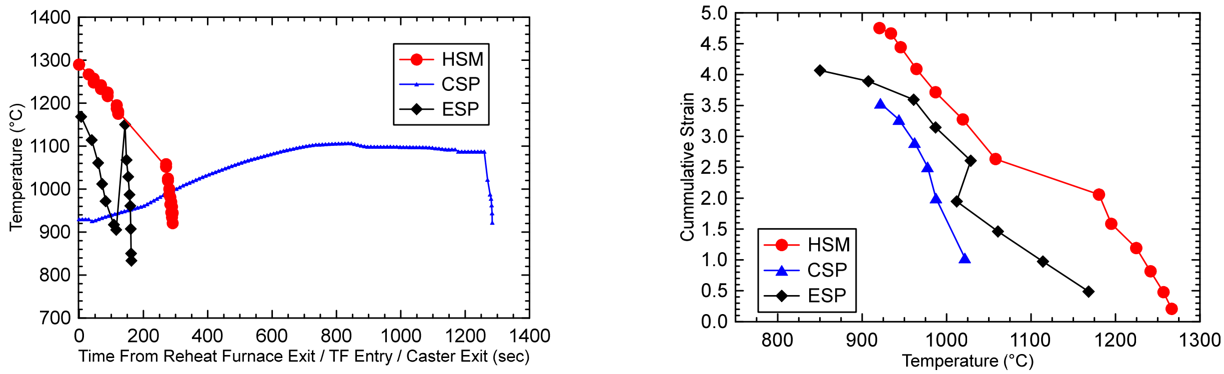

Figure 2. Example of rolling schedules to produce a hot-rolled strip of nominally 2mm thickness with different mill types.

increase considerably. This condition suggests the possibility of early precipitation in niobium and titanium-bearing steels and pancaked austenite in the roughing section.

Figure 3 shows modeled rolling schedules for ESP production based on relatively fast and relative slow casting speeds. The temperature of the last roughing pass differs by more than 100°C in these particular examples. The roughed transfer bars are reheated by induction prior to finish rolling in the Arvedi ESP mill, allowing for adjustable reheating temperature and finish rolling temperatures. In such cases, the reheating time will be relatively short.

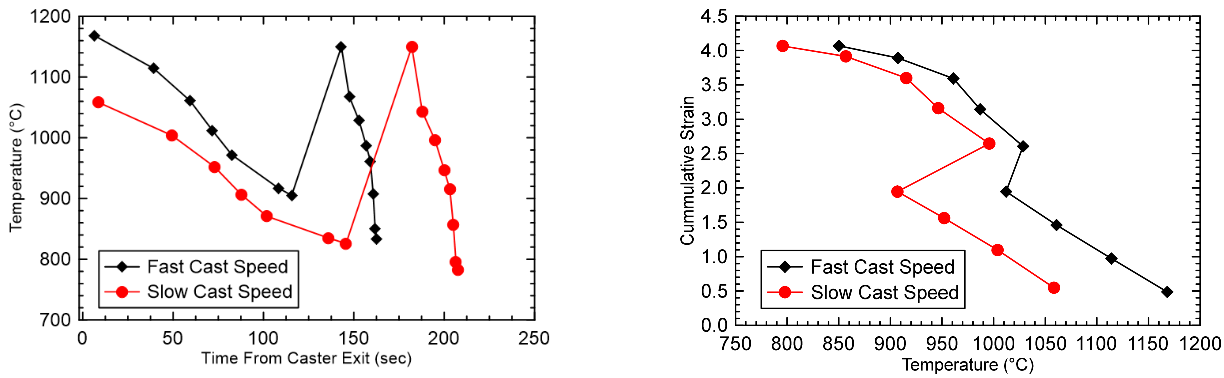

Figure 3. Example of rolling schedules modeled for two different casting speeds in the Arvedi ESP process.

The relatively recent introduction of Arvedi ESP mills leaves some open questions about the specific phenomena occurring upstream of finish rolling. The objective of the current study is to analyze the metallurgical variations in austenite for two microalloyed steels subjected to different rolling conditions that may occur in Arvedi ESP mills. Additionally, the microstructural evolution is modeled using the recently developed MicroSim® Endless version. This tool offers valuable insights for designing and improving endless rolling schedules.

EXPERIMENTAL

Two alloys were selected for this study based on the suspicion of potentially variable austenite and precipitate condition. The chemical composition for each steel is listed in Table I.

Table I. Composition of Experimental Materials (wt. %).

Code	C	Mn	Nb	Ti	Mo	N	Al	P	S
Ti5Nb6	0.057	1.80	0.067	0.047	-	0.006	0.036	0.02	0.003
TiMo	0.048	0.61	-	0.090	0.20	0.004	0.020	0.02	0.006

The Arvedi ESP rolling process was simulated by conducting multipass torsion tests with varying roughing temperatures, induction entry/exit temperatures, and finishing rolling temperatures. Figure 4 illustrates a schematic of the applied rolling schedule and presents the relevant temperatures. Specimens were quenched at positions of interest in the rolling schedule to investigate the evolution of the austenitic structure (see red arrows in Figure 4). Two distinct rolling strategies were defined, referred to as the high T (Schedules 1 and 2) and low T (Schedules 3 and 4) schedules. In the high T rolling schedule, roughing

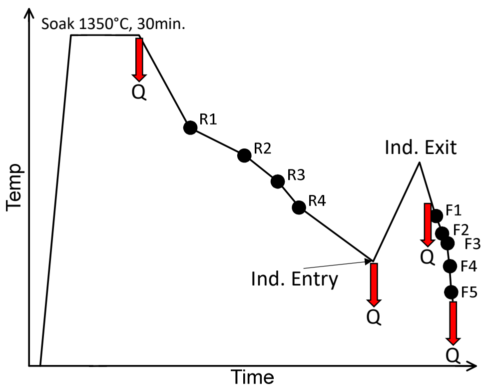

Sched.	Temperature (°C)						Strain per Pass	
	R1	R4	Ind. Entry	Ind. Exit	F1	F5	Roughing	Finishing
1	1168	1012	905	1100			0.64 -> 0.60	
2	1168	1012	905	1200			0.64 -> 0.60	
2+F	1168	1012	905	1200	1063	859	0.64 -> 0.60	0.78 -> 0.22
3	1058	907	825	1100			0.72 -> 0.48	
3+F	1058	907	825	1100	994	844	0.72 -> 0.48	0.84 -> 0.18
4	1058	907	825	1200			0.72 -> 0.48	

Figure 4. Deformation schedules employed to simulate ESP processing with different rolling temperatures and induction heating levels. Red arrows (labeled Q) indication positions where samples were quenched for microstructural analysis.

deformation passes were performed within the 1168-1012ºC temperature interval, whereas in the low T schedule, the four roughing passes were conducted between 1058 and 825ºC. Two induction exit temperatures were selected for the roughing to finishing induction treatment (1100 and 1200ºC). Additionally, finishing deformation passes were applied to extreme cases of high roughing-high induction exit (2+F) and low roughing-low induction exit (3+F) cases.

RESULTS AND DISCUSSION

Austenite Evolution

The evolution of the austenitic microstructure was analyzed by characterizing the austenite at four key stages: (1) prior to roughing deformation (after soaking), (2) after roughing prior to reheating, (3) after reheating prior to finishing deformation, and (4) after finishing deformation. Figure 5 displays the initial austenite structure following the soaking treatment conducted at 1350ºC for 30 minutes for both chemistries. Different initial austenite grain sizes are measured for the two alloys, with the grain size for Ti5Nb6 being finer than that for TiMo. However, it is noteworthy that both alloys exhibit grain sizes finer than what would be expected for an as-cast slab.

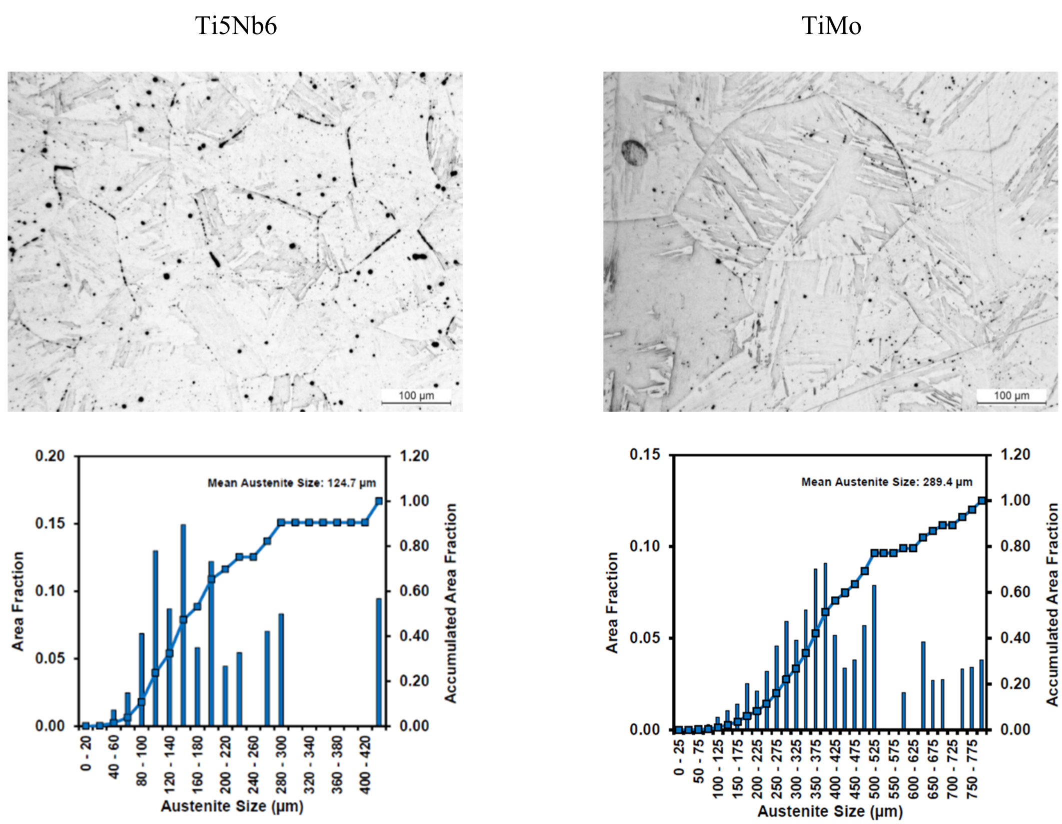

Figure 5. Austenite grain size after soaking treatment of 1350°C for Ti5Nb6 and TiMo steels.

Figures 6 and 7 show the evolution of grain structure as a function of the rolling strategy for Ti5Nb6 and TiMo alloys, respectively. When the high T rolling schedule is applied, similar austenite grain size evolution is observed for Ti5Nb6 and TiMo steels. Both steels have a fine, fully recrystallized austenite structure prior to reheating. By contrast, with lower roughing temperature the austenite is heavily pancaked after the roughing stage and before entering the induction treatment for both steels. The pancaked austenite grains are thinner for Ti5Nb6 than TiMo suggesting recrystallization is interrupted earlier for the Nb-bearing steel. In spite of the pancaked structure obtained after roughing, the induction treatment promotes the activation of static recrystallization leading to a fully equiaxed structure after reheating in both steels. Finally, the microstructure is pancaked after finishing passes in both steels and rolling strategies.

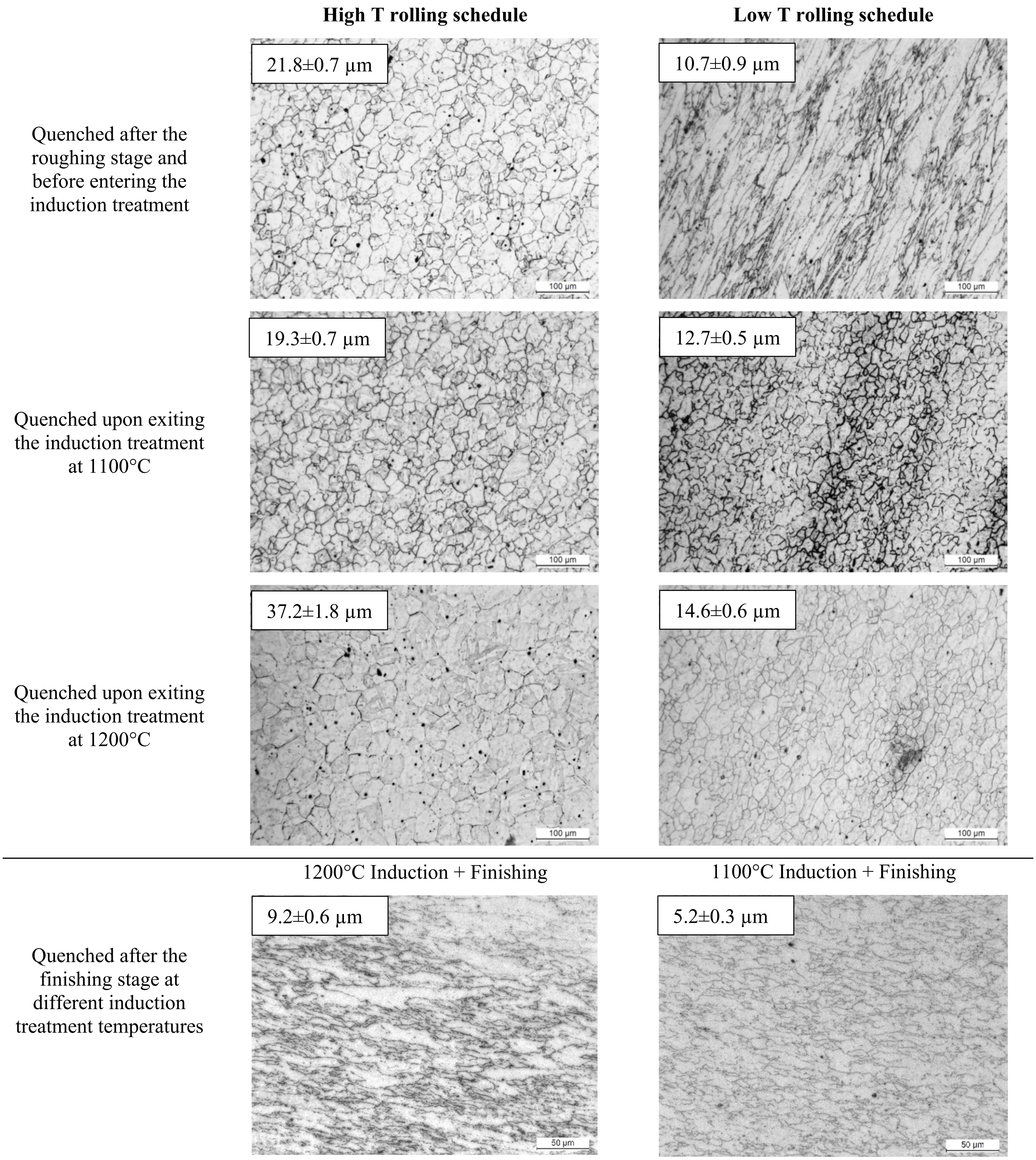

Figure 6. Evolution of the austenite grain structure for Ti5Nb6 steel processed with the schedules illustrated in Figure 4.

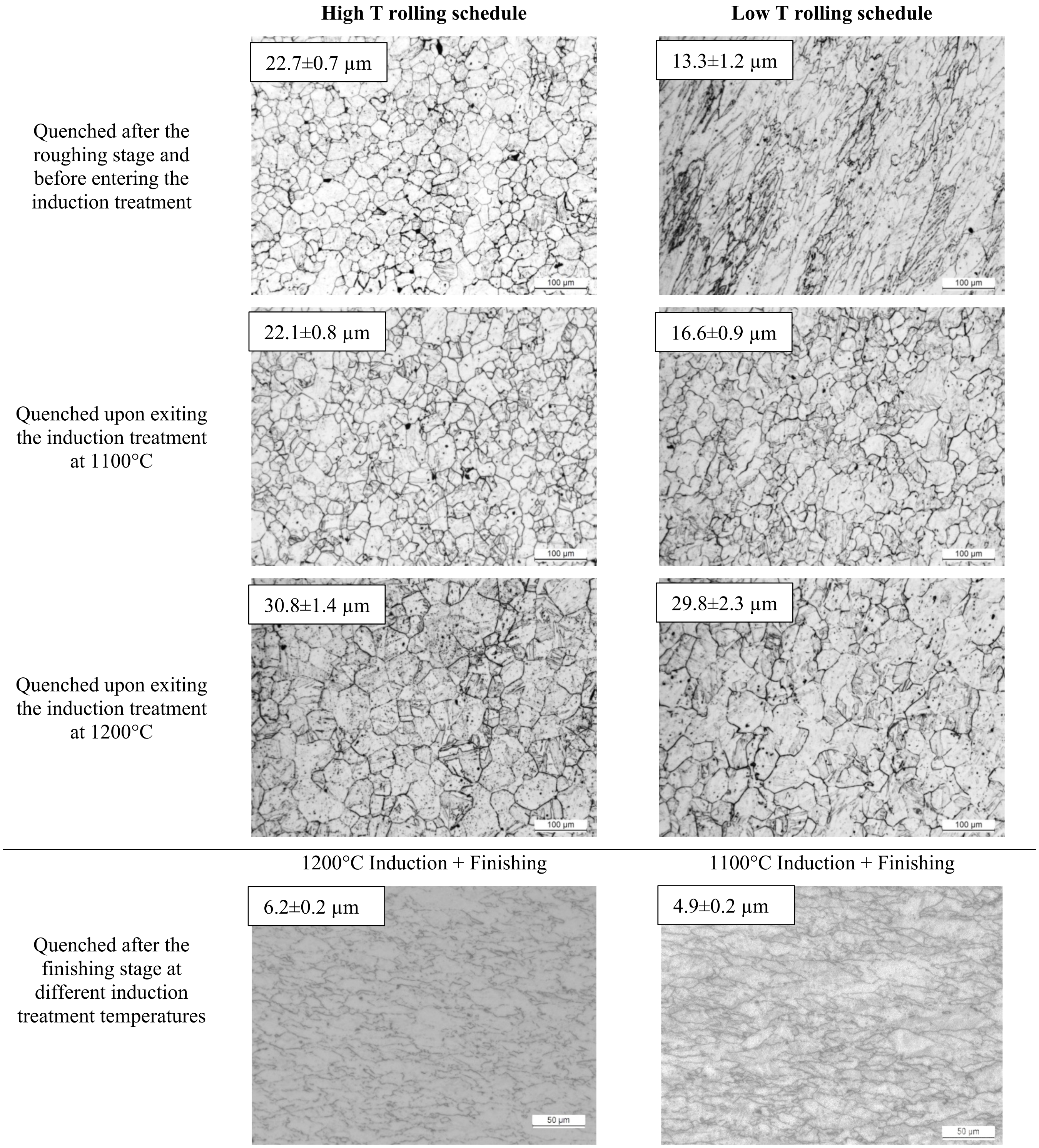

Figure 7. Evolution of the austenite grain structure for TiMo steel processed with the schedules illustrated in Figure 4.

Impact of the Induction Exit Temperature

Figure 8 summarizes the observed austenite grain size evolution. It is clear that the difference in grain size after soaking was eliminated by the roughing deformation. At this stage, both alloys have similar austenite grain size which was dictated by the rolling schedule (approximately 22 µm and 12 µm for high and low T schedules, respectively). However, the response to the different induction heating temperatures varied depending on the chemistry and rolling schedule. Consider first the 1100°C reheating condition. Fine and recrystallized austenite is observed for both steels and rolling schedules, with similar austenite grain sizes at the entry and exit of the induction treatment. By contrast, differences become evident when the 1200°C reheat is applied. Under the high T rolling schedule, grain growth is observed in both steels, with somewhat greater growth observed in

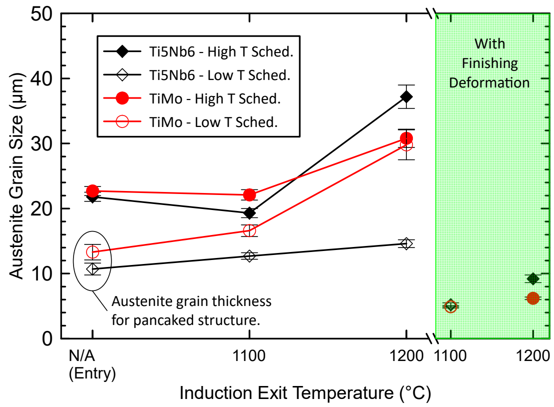

Figure 8. Evolution of the austenite grain size as a function of induction heating temperature.

Ti5Nb6 steel (grain size increases from 22.7 µm to 30.8 µm for TiMo steel and from 21.8 µm to 37.2 µm for Ti5Nb6 chemistry). Conversely, for the low T rolling schedule, while TiMo steel demonstrated growth to a grain size similar to its high T schedule counterpart, Ti5Nb6 steel exhibited very limited growth. It seems that there is an effective control of grain growth when the Ti5Nb6 steel is subjected to the low T rolling schedule. This phenomenon could be linked to the precipitation of (Nb,Ti)C precipitates, which have the potential to act as grain growth inhibitors. In the subsequent paragraphs, Thermocalc simulations will be integrated with TEM (Transmission Electron Microscopy) analysis to gain insights into these behaviors.

Figure 9 presents Thermocalc (version 2020b with TCFE9 database) prediction results of the precipitate fraction and alloying elements in solution for Ti5Nb6 and TiMo steels. By the time the transfer bar reaches the induction heating system, it will have cooled to a temperature where significant precipitation may occur in both steels, and the roughing deformation could serve to stimulate these reactions. For Ti5Nb6 steel, Thermocalc predicts the initial formation of TiN-rich precipitates followed by (Nb,Ti)C precipitates, the later ones affecting the austenite microstructural evolution (see Figure 9-a). By contrast, for TiMo steel, TiC and coarse TiN particles are expected to precipitate, which are not expected to be as influential during high temperature rolling as the (Nb,Ti)C precipitates in steel Ti5Nb6. Additionally, different induction reheating temperatures would result in different degrees of precipitate dissolution, as shown in Figure 9-b. In the case of Ti5Nb6 chemistry, noticeable variations in the fractions of Nb and Ti in solution are observed depending on the chosen induction exit temperature. When an induction exit temperature of 1100ºC is employed, Thermocalc predicts a substantial presence of Nb- and Ti-rich precipitates within the austenitic matrix. Conversely, increasing the induction exit temperature to 1200ºC, it appears that a majority of the Nb- and Ti-rich precipitates are dissolved, and the critical element Nb is completely in solution.

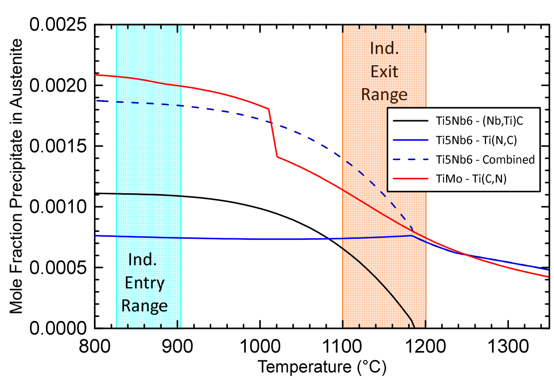

(a)

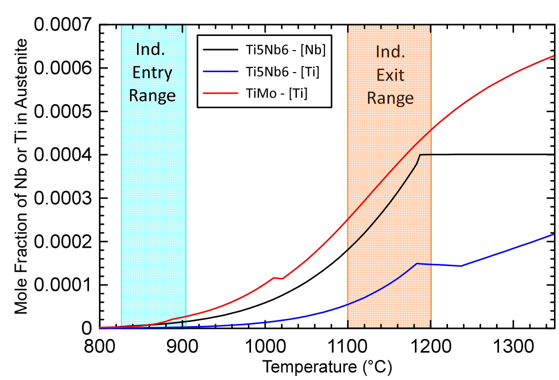

(b)

Figure 9. Thermocalc prediction of (a) precipitate amount and (b) alloying elements in solution in austenite, across the hot rolling interval.

To characterize the precipitation pattern predicted by Thermocalc on the Ti5Nb6 chemistry, a TEM analysis was conducted using carbon extraction replicas. Samples following the low-T rolling schedule and quenched at both the entry and exit of the induction treatment performed at 1200°C were chosen for the analysis (see Figure 10). TEM micrographs corresponding to the sample quenched at the entry of the induction heating treatment confirm the predictions of Thermocalc in Figure 9, revealing a fine precipitation of Nb-Ti rich particles.

Quenched after the roughing stage and before entering the induction treatment

Quenched upon exiting the induction treatment at 1200°C

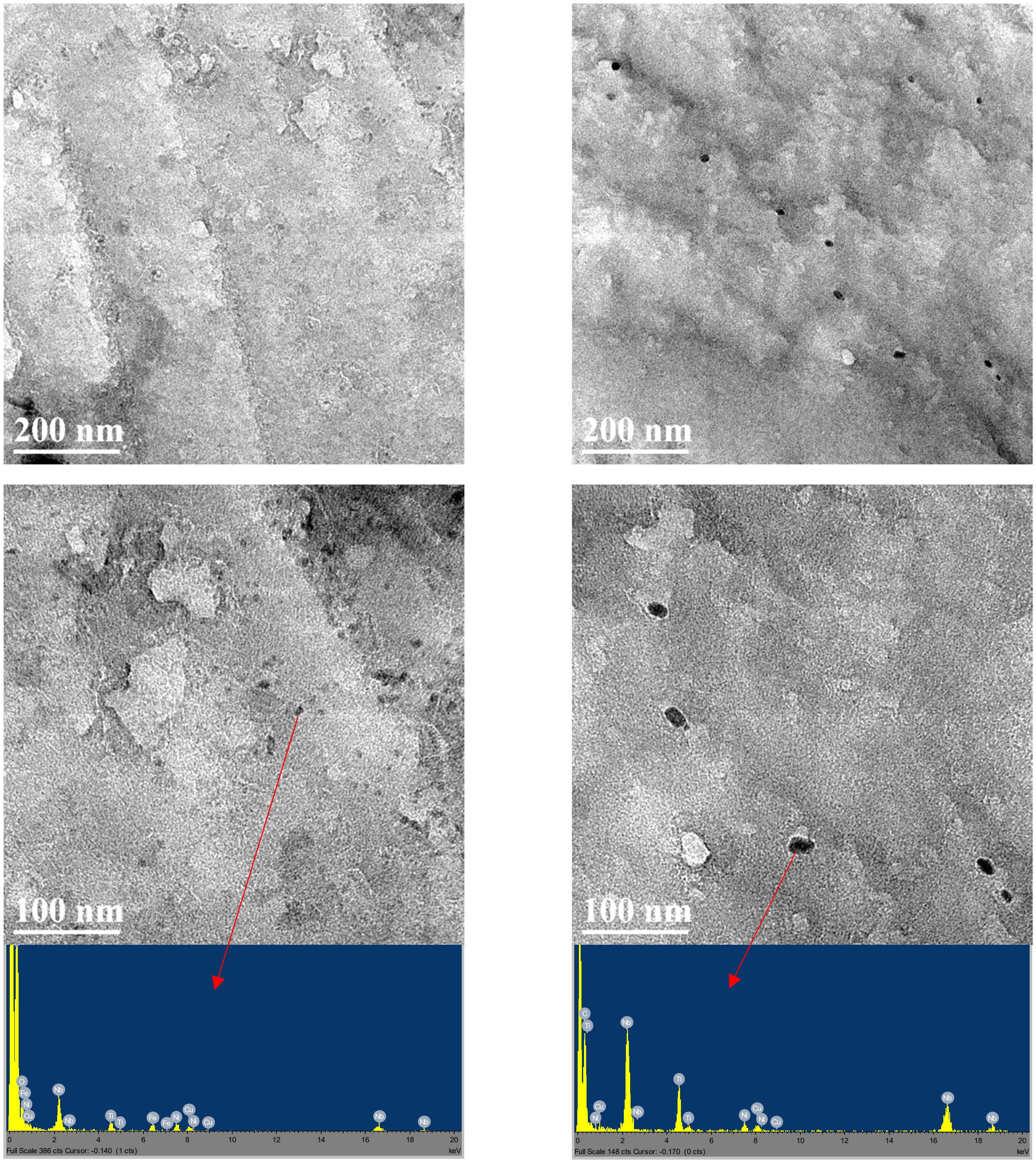

Figure 10. TEM micrographs illustrating the presence of fine Nb-Ti rich precipitates for different stages of the ESP processing on the Ti5Nb6 steel.

After the induction heating treatment performed at 1200ºC, a significant coarsening and dissolution of the Nb-Ti precipitates is observed (see Figure 10). However, some Nb-Ti precipitates remain. These TEM observations differ from the Thermocalc estimation that (Nb,Ti)C is dissolved at 1200ºC. Considering the observed control over grain growth in the low-T rolling schedule for Ti5Nb6 steel (see Figure 8), it is evident that the remaining precipitation, despite some coarsening, still has the capability to inhibit the austenite grain growth at 1200ºC. It is noted that the relatively short times of the induction heating step are far from the equilibrium conditions assumed by Thermocalc and dissolution kinetics must be considered.

Validation of MicroSim® Endless

A version of MicroSim® Endless model, customized for the Arvedi ESP configuration was developed. This model predicts the evolution of the austenite grain size distributions during the rolling process. The Arvedi ESP customized version takes into account the specific grain growth characteristics during the intermediate induction heating process and has been validated by laboratory torsion multipass tests. Figure 11 shows the comparisons between the model predictions and the experimental measurements, focusing on the high-temperature roughing cycles for both steels. From the figure it is clear that the grain size distribution for Ti5Nb6 and TiMo steel is nicely predicted for these schedules.

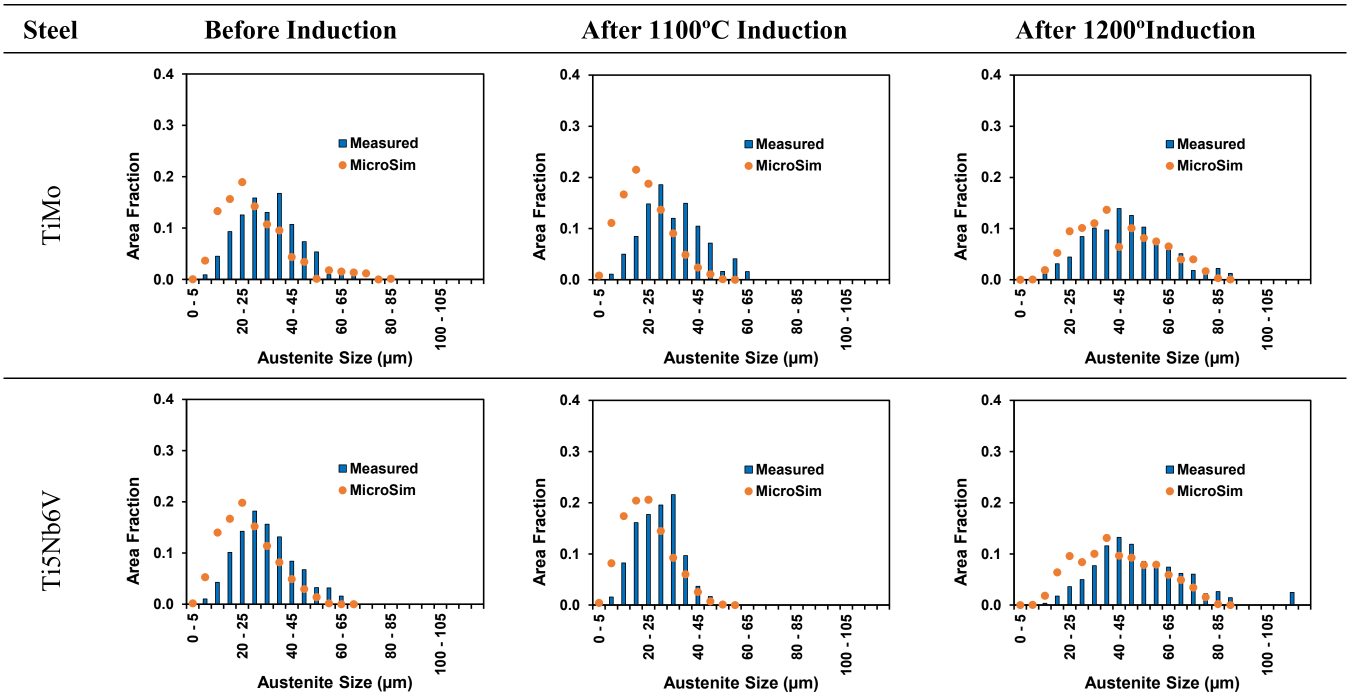

Figure 11. Comparison between torsion test measurements and MicroSim® Endless predictions for the high temperature roughing schedules.

Similarly, Figure 12 depicts the comparisons between the model predictions and the experimental measurements for low temperature roughing cycles performed in the Ti5Nb6 chemistry. As for high-T schedule, the model predictions for the low temperature cycles go in the same direction except for one case. The grain size distribution is correctly predicted after the 1100ºC peak temperature, but the model predicts an excessively coarse microstructure after the 1200ºC reheating temperature when compared to the experimental measurements. Based on the predictions of the model, the microstructure remains unrecrystallized before the induction reheating and strain induced precipitates are formed starting after the first roughing pass. Even if fine precipitates are formed during roughing passes, the microstructure fully recrystallizes during reheating (as shown in Figure 6). Therefore, it seems that the Nb(C,N) precipitates formed during roughing do not prevent recrystallization during reheating, but can control grain growth and final gran size. This effect will be included in future versions of the software. Additional laboratory tests will be designed to confirm this behavior under different conditions and chemical compositions.

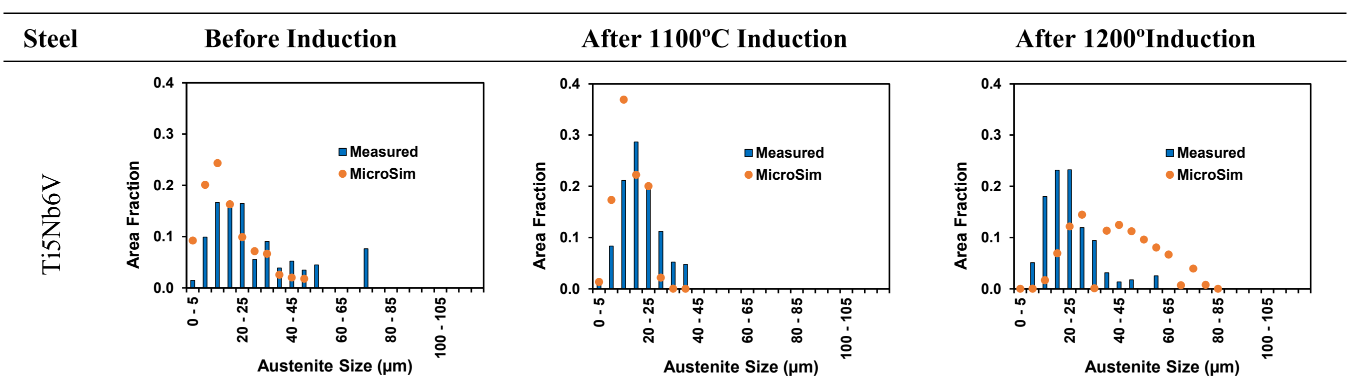

Figure 12. Comparison between torsion test measurements and MicroSim® Endless predictions for the Ti5Nb6 steel and the low temperature roughing cycle.

Figure 13 shows the comparison between the measured microstructures and MicroSim predictions after finishing passes.. In most of the cases the predictions are quite accurate, with MicroSim predicting somewhat finer grain size than was observed experimentally (particularly for the case of low roughing and 1100ºC peak temperature in the Ti5Nb6 steel).

Steel	After Finishing - Low T Roughing + 1100ºC Induction	After Finishing - High T Roughing + 1200ºC Induction
TiMo	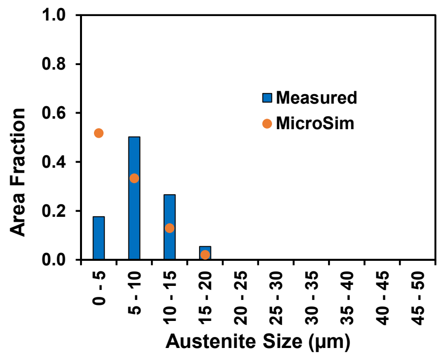	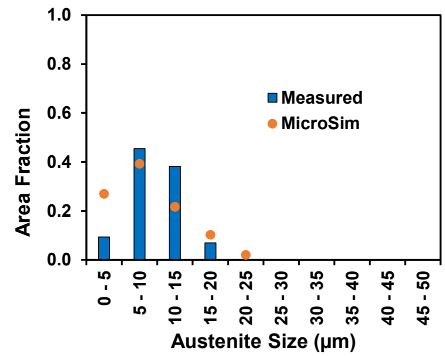
Ti5Nb6V	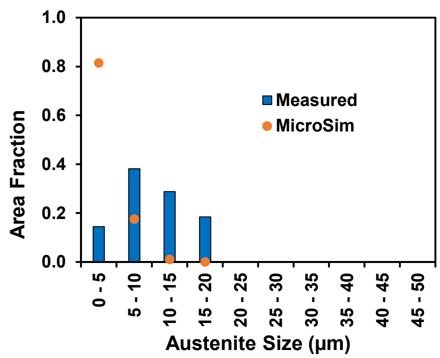	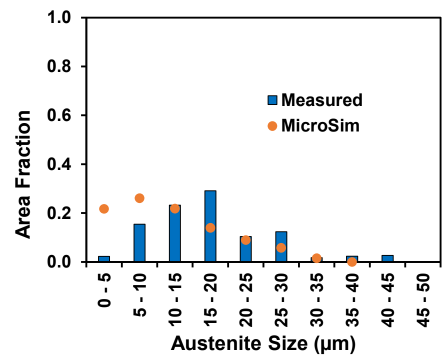

Figure 13. Comparison between torsion test measurements and MicroSim® Endless predictions after finishing passes.

Simulation of Industrial Rolling Sequences using MicroSim® Endless

As stated previously, the laboratory simulation produced an initial grain size after soaking that was significantly finer than expected in an as-cast slab. The initial austenite grain size differences are especially relevant when considering roughing conditions where recrystallization may be incomplete. In the current study, the lower roughing temperatures would be closer to those situations. Several simulations were run using MicroSim® Endless with initial grain size distribution representing industrially cast slabs with an average of about 1000 µm and a maximum grain size of 2400 µm [11]. Figures 14 and 15 show the predicted austenite grain size distributions for high and low temperature roughing conditions, respectively. The color code refers to the nature of each austenite family. The recrystallized grains are plotted in blue, the unrecrystallized grains due to solute drag are plotted in yellow, and the unrecrystallized grains due to strain induced precipitation are shown in red.

For the TiMo steel, results of MicroSim simulations performed with industrial as-cast grain size (see Figure 14 and Figure 15) are similar to those obtained using the grain size from the torsion test soak condition (plotted in Figure 11). Therefore, the impact of the initial grain size distribution from the as-cast condition entering the roughing stands doesn't affect the microstructural evolution significantly. The repeated recrystallization steps produce refined and homogenized microstructure entering the induction reheating stage in all cases.

For the Ti5Nb6 steel though, the behavior is different when compared to the torsion test samples. When the Low-T schedule is applied, strain induced precipitation of Nb(C,N) is activated and the initial coarse as-cast microstructure remains unrecrystallized from pass to pass. This results in a heterogeneous structure at the entry to the induction heating stage (see Figure 15). The model predicts that all this heterogeneity will disappear and fully homogeneous microstructure will be formed after both reheating temperatures. There is not yet experimental evidence that induction reheating cycles would be able to completely refine a very heterogenous microstructure with grains in the 400-500 µm range. This effect should be analyzed in more detail as this work has shown the model to underpredict the influence of persistent (Nb,Ti)C particles in the Ti5Nb6 steel.

Special care should be taken in rolling schedules with very low roughing temperatures as heterogeneity remaining after roughing could impair the homogeneity of the microstructure entering the finishing stands.

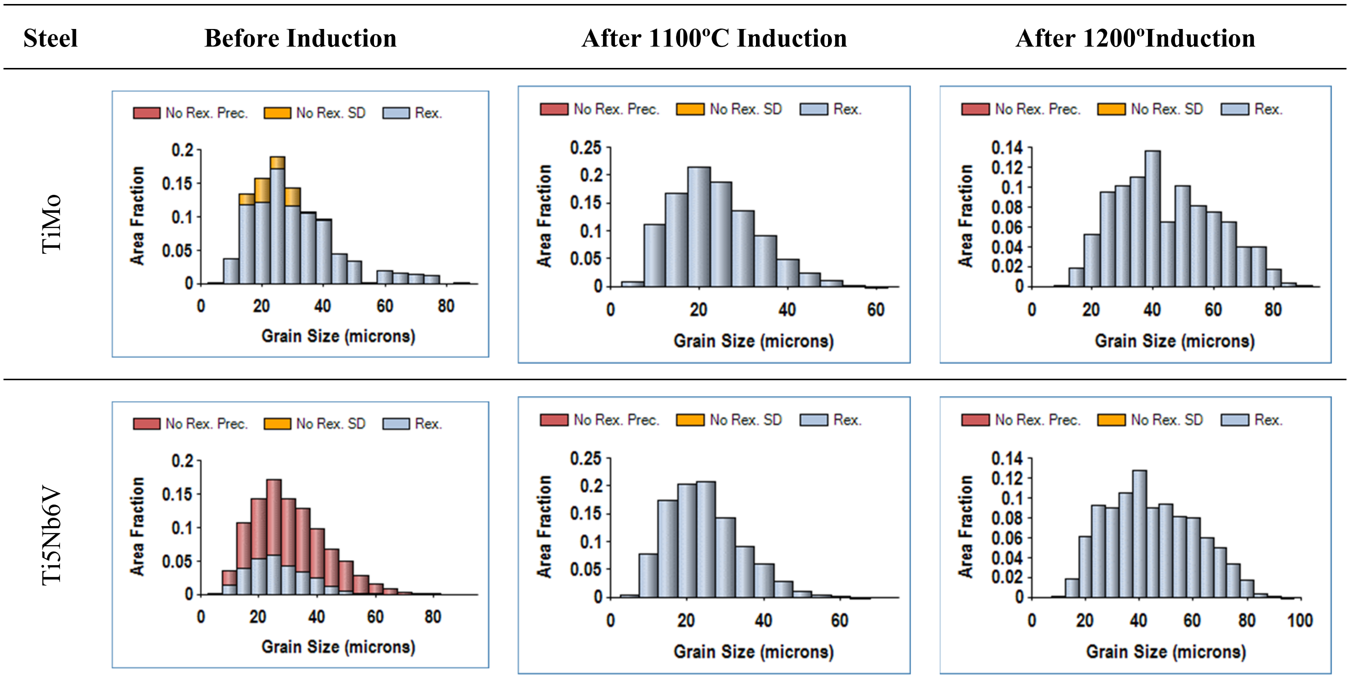

Figure 14. MicroSim® Endless predictions for the high temperature roughing schedules considering industrial casting and rolling conditions.

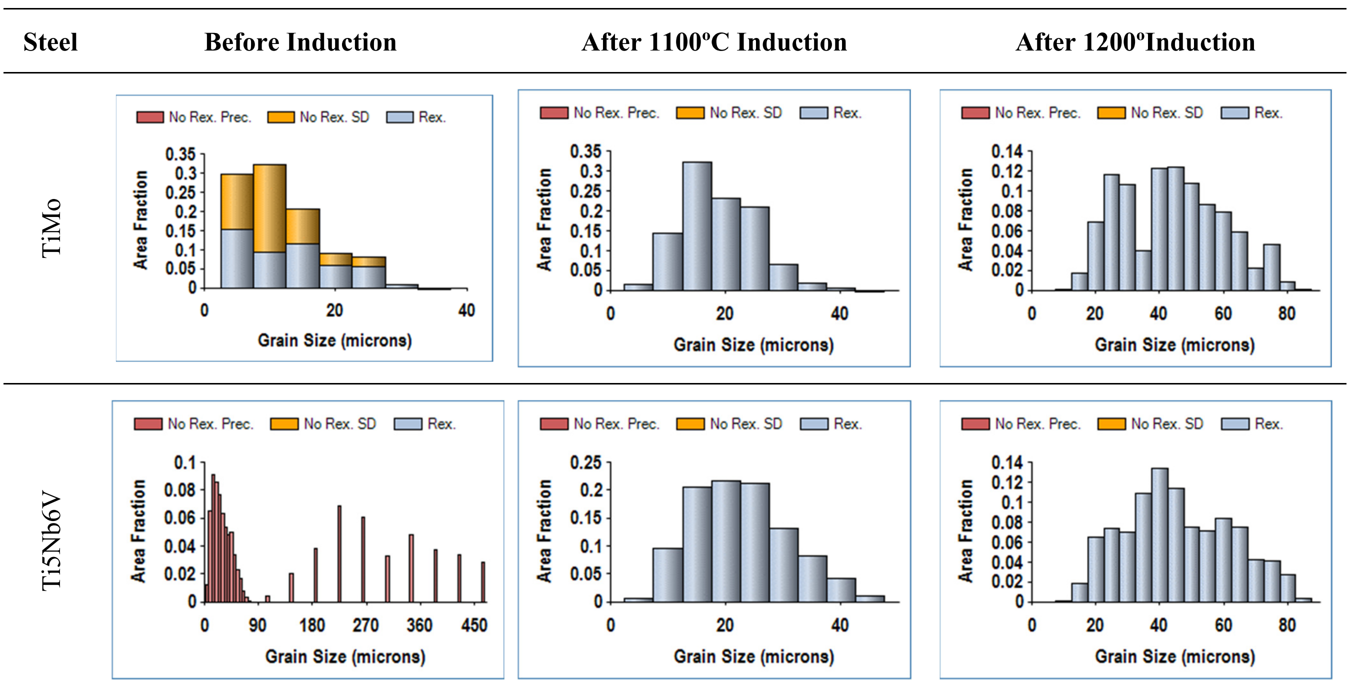

Figure 15. MicroSim® Endless predictions for the low temperature roughing schedules considering industrial casting and rolling conditions.

Figure 16 shows some simulation results of MicroSim® Endless focused on the recrystallization behavior and austenite grain size distributions after the finishing stands. The charts in the figure are generated by the Compare tool within MicroSim. Two main trends can be highlighted from the figures. Schedules 1 and 3, which are the ones with the 1100ºC induction peak temperature, result in a more pancaked microstructure. This is attributed to the application of lower finishing temperatures, leading to a higher proportion of unrecrystallized fraction throughout the finishing passes. The strain induced precipitation of Nb(C,N) during finish rolling in the Ti5Nb6 steel amplifies this effect, with full strain accumulation occurring in all cases during the final 3-4 passes. The lower temperatures in the finishing passes also result in a finer microstructure for both steels. For schedules 2 and 4, with an induction peak temperature of 1200ºC, though, the evolution of the microstructure during the finishing passes results in a coarser microstructure with a considerably lower pancaking due to the fact that most passes during finishing promote a mixed microstructure between recrystallized and unrecrystallized grains. These mixed structures might result in more heterogeneous microstructures at the exit of the finishing mill.

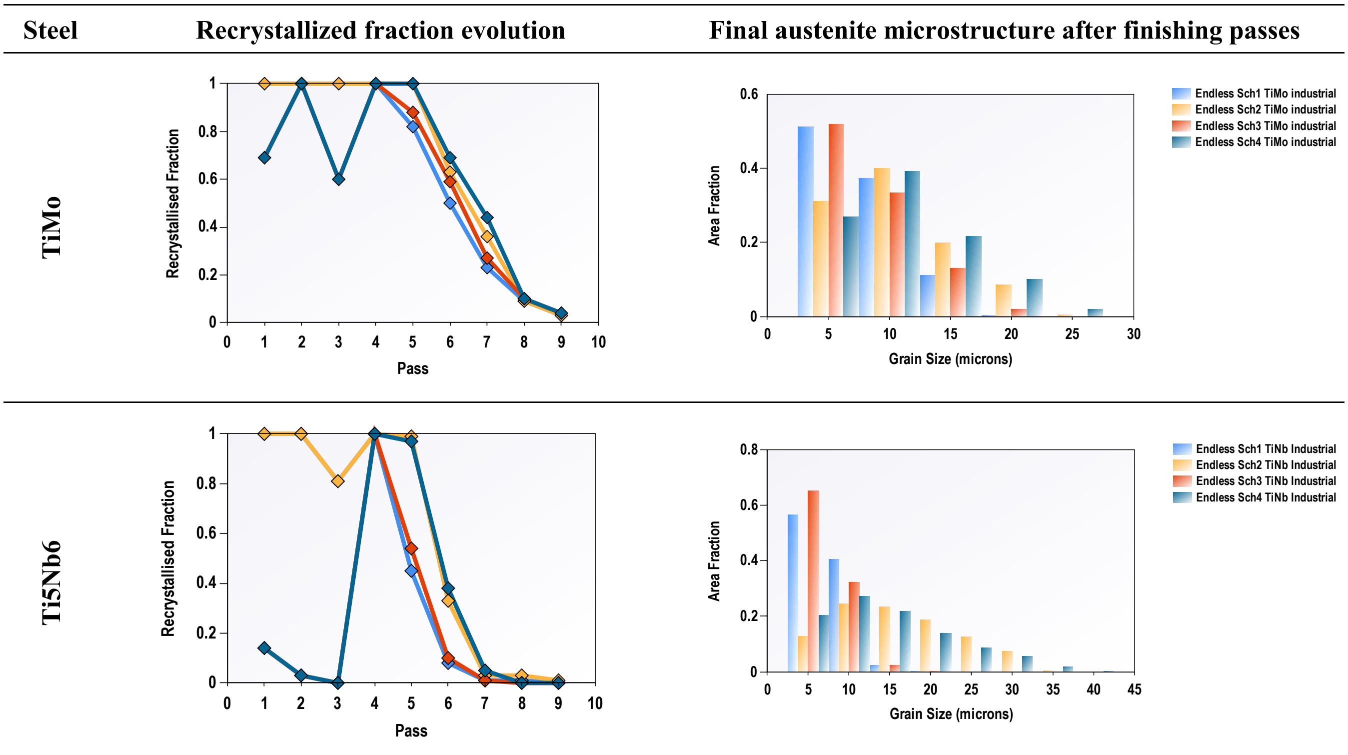

Figure 16. MicroSim® Endless predictions using the Compare tool showing the evolution of recrystallized fraction during roughing and finishing as well as the final austenite grain size distributions after the finishing passes.

This analysis shows the relevance of a suitable parameter configuration to balance on one side the casting speed, resulting in higher or lower roughing temperatures, and the peak temperature during induction heating, as this might affect grain size distribution entering finishing stands and the evolution of the microstructures until final transformation. As a general rule, and depending on the steel grade being rolled, the first step should be to ensure full recrystallization during roughing, avoiding premature carbonitride precipitation and blockage of further recrystallization. This should be coupled with an appropriate induction cycle to optimize microstructural evolution during the last passes, increasing the austenite conditioning through pancaking and avoiding mixed microstructure formation to maximize microstructural refinement and homogeneity after phase transformation during cooling.

CONCLUSIONS

This study highlights variations in the austenite condition of microalloyed steels that can arise from different operating conditions in a directly-coupled casting and rolling operation. Differences in casting speed can lead to varying temperatures in the rough rolling section, influencing precipitation reactions and whether the austenite recrystallizes before transfer bar reheating. Fine Nb-Ti precipitates induced by low temperature rough rolling were found to persist even with 1200°C transfer bar reheating. These particles restricted austenite grain growth, but did not prevent static recrystallization under the experimental conditions.

Complex interaction between strain induced precipitation and recrystallization phenomena were detected in the study. Even if further research would be needed, special attention should be paid to slow casting speeds with highly microalloyed grades, as the consequently low roughing temperature might impact final homogeneity and mechanical properties such as ductility or toughness. The intermediate induction treatments seem to be a very effective metallurgical tool in order to increase homogeneity in the microstructure before entering the finishing stands. Even after high finishing entry temperatures, pancaked final microstructures, with fine and homogeneous distributions are achieved, leading to presumably fine and homogeneous final microstructures after transformation.

ACKNOWLEDGEMENTS

The authors are thankful for the contribution of Primetals Technologies, particularly S. Grosseiber, for providing the representative rolling schedules of the Arvedi ESP process described herein.

DISCLAIMER

The material in this paper is intended for general information only. Any use of this material in relation to any specific application should be based on independent examination and verification of its unrestricted availability for such use and determination of suitability for the application by professionally qualified personnel. No license under any United States Steel Corporation patents or other proprietary interest is implied by the publication of this paper. Those making use of or relying upon the material assume all risks and liability arising from such use or reliance.

REFERENCES

1. C. Bilgen, C. Klein, C. Klinkenberg, J. Müller, Procs. AISTech 2012 Conf., AIST, 2012, pp 1339.
2. C. Klinkenberg, C. Bilgen, C. Klein, A. Meyer, J. Müller, Steel Times International, 37, 2013, pp 40.
3. A. Pigani, P. Bobig, M. Knights, M. Knigge, Procs. AISTech 2019 Conf., AIST, 2019, pp 1395.
4. J. Müller, C. Fröhling, F. Seuffert, Procs. AISTech 2020 Conf., AIST, 2020, pp 908.
5. L. Faralli, Procs. AISTech 2023 Conf., AIST, 2023, pp 705.
6. G. Arvedi, F. Mazzolari, J. Siegl, G. Hohenbichler, G. Holleis, Ironmaking Steelmaking, 37, 2010, pp 271.
7. R. Venturini, P. D. Avancini, N. Barbier, A. Rizzi, Mater. Sci. Forum, 854, 2016, pp 42.
8. B. Linzer, A. Jungbauer, Mater. Sci. Forum, 854, 2016, pp 207.
9. "US Steel invests in Primetals ESP line," Steel Times International, 43 no.4, 2019, pp 6.
10. "Building the Nation's Most Technologically Advanced Steelmaking Facility in Osceola, Arkansas," United States Steel Corporation presentation to investors, January 11, 2022.
11. P. Uranga, A.I. Fernández, B. López, J.M. Rodriguez-Ibabe, 43rd Mechanical Working and Steel Proc. Conf., ISS, Charlotte, USA, 39, 2001, p 511.

